applied sciences

MDPI

Article

Deadbeat Predictive Current Control for Circulating Currents Reduction in a Modular Multilevel Converter Based Rail Power Conditioner

Mohamed Tanta [1,*], J. G. Pinto [1], Vitor Monteiro [1], Antonio P. Martins [2], Adriano S. Carvalho [2] and Joao L. Afonso [1]

[1] Campus of Azurém, University of Minho, 4800-058 Guimarães, Portugal; gpinto@dei.uminho.pt (J.G.P.); vmonteiro@dei.uminho.pt (V.M.); jla@dei.uminho.pt (J.L.A.)

[2] University of Porto, Rua Roberto Frias, 4200-465 Porto, Portugal; ajm@fe.up.pt (A.P.M.); asc@fe.up.pt (A.S.C.)

* Correspondence: mtanta@dei.uminho.pt; Tel.: +351-253-510-190

Received: 31 January 2020; Accepted: 3 March 2020; Published: 8 March 2020

Abstract: This paper presents a deadbeat predictive current control methodology to reduce the circulating currents in a modular multilevel converter (MMC) when it operates as a rail power conditioner (RPC) in a conventional railway system-based V/V connection. For this purpose, a half-bridge MMC based on half-bridge submodules, operating as an RPC is explained, and the total system is denominated as a simplified rail power conditioner (SRPC). The SRPC in this study is used to compensate harmonics, reactive power, and the negative sequence component of currents. This paper explains the SRPC system architecture, the key control algorithms, and the deadbeat predictive current control methodology. Mathematical analysis, based on the MMC equivalent circuit, is described and the reference equations are presented. Moreover, simulation results of the deadbeat predictive current control methodology are compared with the results of the conventional proportional-integral (PI) controller. This comparison is to verify the effectiveness of the proposed control strategy. Simulation results of the SRPC show reduced circulating currents in the MMC phases when using the predictive control approach, besides accomplishing power quality improvement at the three-phase power grid side.

Keywords: circulating current; deadbeat predictive current control; modular multilevel converter (MMC), rail power conditioner (RPC)

1. Introduction

Power quality phenomena in alternating current (AC) electrified railway have drawn more attention in the last decades, especially, after the evolution in the power electronics field [1]. Railway operators have an absolute interest to run the electrified trains with the lowest possible costs. In this context, various solutions were proposed to overcome the power quality deterioration in the electrified railway, e.g., the flexible AC transmission systems (FACTS) presented in [1–5]. On the other side, the modular multilevel converter (MMC) is an attractive solution for medium-voltage applications due to the lower harmonics, lower switching losses, MMC flexibility, and scalability [6,7] since other multilevel converters, such as the neutral point clamp and the flying capacitor multilevel converters, are quite hard to extend to higher levels [8]. Therefore, MMC has been enhanced to be combined with the FACTS family. As example, MMC has been dedicated to operating as a rail power conditioner (RPC) with different topologies in [6,9], and an MMC based static synchronous compensator for railway applications is proposed in [10].

Half-bridge converters have been used in high power applications due to their high efficiency, low cost and simple control compared to the full-bridge converters [11]. In this context, the half-bridge

AC/DC/AC MMC based RPC using a V/V power transformer, denominated as a simplified rail power conditioner (SRPC), is used in this study. The main disadvantage of the half-bridge MMC is the fact that it requires the double of the voltage with respect to the output neutral, and therefore, two capacitors with a mid-neutral point are required. In any case, the SRPC total power rating is divided between the MMC submodules (SMs), then, a higher number of MMC SMs signifies lower power ratings required for each SM, and a better output performance to synthesize a multilevel output waveform. A SM consists of a storage capacitor (with voltage V_{SM}) and a half-bridge converter [12].

The circulating current control is important to suppress the harmonic contents produced in the MMC arm currents due to the SM capacitor voltage ripples or the inner DC-voltage differences between the MMC SMs. The magnitude of the circulating current has an influence on the MMC arm current. It increases the total root mean square (RMS) values of the MMC arm currents, which leads to extra power losses, and second-order harmonics will result in further generation of other higher-order harmonics, such as the 4th, 6th, 8th, etc., [13]. The circulating currents do not contribute to the MMC output currents synthesized by the power compensator, since the circulating currents flow only in the MMC arms [14].

As a conventional method to suppress circulating currents, inner passive filters are used, but they do not totally solve the circulating currents problem [15]. Furthermore, the large passive component values may lead to bulky implementation of the MMC [16]. The circulating current can be reduced by increasing the inductors between the MMC arms or by increasing the SM capacitor. Nevertheless, the size of the inductors and the cost of SM capacitors have to be taken into account [17]. On the other hand, as addressed in [18], the existence of a small circulating current component in the MMC arm current can be useful to have a control freedom, thus optimizing the MMC performance. In some applications, circulating currents can be used in a useful way, e.g., during the phase-to-ground fault, in which the MMC works in an asymmetrical operation whereby the power will flow through the upper and the lower MMC arms, leading to an imbalance of arm capacitor energy. In that case, improved control strategies were developed based on circulating current injection [19,20].

Concerning the circulating current elimination, a method based on repetitive controller and proportional-resonant (PR) controllers using a phase-shifted pulse-width modulation (PWM) is presented in [8]. In addition, and as presented in [21], a proportional-integral (PI) controller is used to control the circulating current. However, many variables have to be well-adjusted to guarantee a good circulating current cancellation. In particular, a method based on a dual vector current controller for high-voltage direct current systems under unbalanced voltage conditions is presented in [21,22]. However, under unbalanced voltages, the circulating current is composed of positive sequence component, negative sequence component (NSC), and zero sequence component. Hence, this method is not the most adequate for the SRPC application, since the converter is used for the purpose of active power balancing and reactive power compensation in two-phase V/V connection. On the other hand, a model predictive control for circulating current suppression is proposed in [23]. However, when increasing the number of SMs in an MMC, this leads to a higher number of switching states, which increases the control complexity due to the massive calculations that could overload the digital controller [24]. A new method for reducing the circulating current by adding second and fourth harmonics in the upper and the lower MMC arm currents is presented in [7]. However, this method does not eliminate all the even-order harmonics in the MMC arm currents.

In this context, a methodology using the deadbeat predictive current control to reduce the MMC circulating currents is presented in this paper, bearing in mind that, the interrelation between the MMC output currents, the MMC circulating currents, and the SM voltages complicates the MMC control. Moreover, these quantities could affect each other, thus affecting the MMC performance [14]. The deadbeat predictive control uses the model of the SRPC system to compute, during every sampling period, the required reference voltage that the converter needs to reach the reference value in the next sampling instant [25]. Therefore, studying the SRPC model is important to extract the reference voltages. Then, the output voltage signal of the deadbeat predictive controller is compared with a

phase-shifted PWM to drive the switching devices. Indeed, the more accurate the parameter values of the SRPC model, the better the performance of the controller.

In this framework, the main contributions of this paper are: (a) Proposing a methodology based on a deadbeat predictive current control for the circulating current suppression in MMC; (b) An ample mathematical analysis of the SRPC equivalent circuit to extract the final reference equations; (c) A comprehensive comparison between the deadbeat predictive current control methodology and the conventional PI control approach.

This paper is organized as follows: Section 2 explains the SRPC system compensation principle when using the V/V power transformer connection. Section 3 presents in detail the SRPC mathematical analysis based on the MMC equivalent circuit to extract the final reference voltages. Section 4 presents the control algorithm blocks of the SRPC system, including, the MMC voltage balancing control. Section 5 presents the simulation results and, finally, Section 6 summarizes the main conclusions.

2. SRPC Compensation Principle

The SRPC system structure is presented in Figure 1, where the main objective is to compensate the NSC of currents, besides the harmonics produced by the electric locomotives [6]. A higher current imbalance ratio indicates a huge difference between the three-phase currents and a higher NSC of currents injected into the three-phase public power grid. The right feeder section is denoted as phase x and the left feeder section is denoted as phase y. The corresponding phases on the primary side windings of the V/V power transformer are denoted as phase A and phase B, respectively. By considering the three-phase power grid voltages $\dot{U}_A$, $\dot{U}_B$, and $\dot{U}_C$ are:

$$\begin{aligned} \dot{U}_A &= U_A\, e^{\,j0^\circ} \\ \dot{U}_B &= U_B\, e^{-j120^\circ} \\ \dot{U}_C &= U_C\, e^{-j240^\circ} \end{aligned} \tag{1}$$

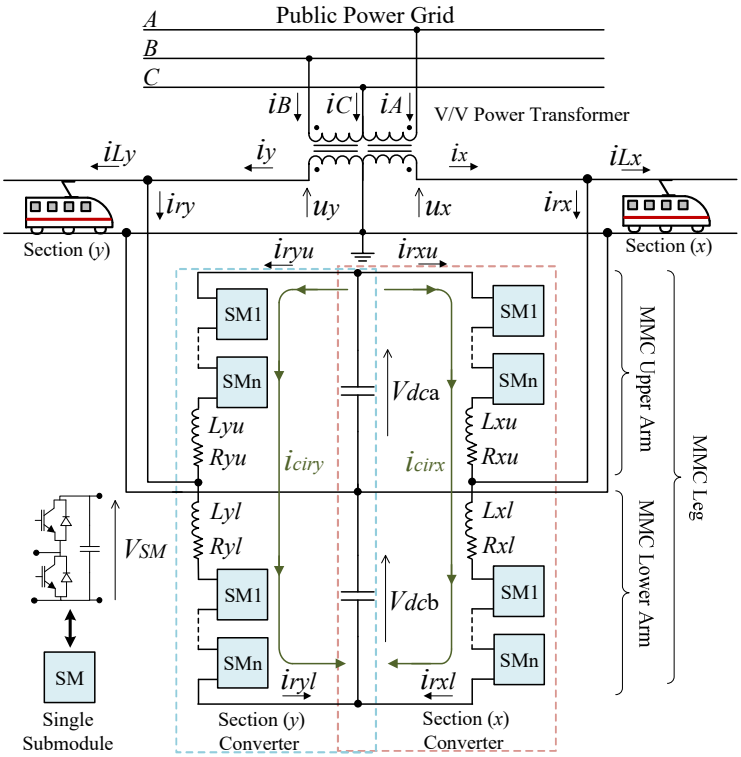

Figure 1. Structure of the half-bridge modular multilevel converter (MMC) based simplified rail power conditioner system (SRPC) used to validate the proposed control strategy.

From Equation (1), and as shown in Figure 1, phase x and phase y voltages, $\dot{U}_x$, $\dot{U}_y$ of the traction power system correspond to the line-to-line grid voltages of $\dot{U}_{AC}$, and $\dot{U}_{BC}$, respectively, and can be expressed as in Equation (2).

$$\begin{aligned} \dot{U}_x &= \tfrac{U_{AC}}{K_V}\, e^{-j30^\circ} \\ \dot{U}_y &= \tfrac{U_{BC}}{K_V}\, e^{-j90^\circ} \end{aligned} \tag{2}$$

where, K_V, denotes the turns ratio of the V/V power transformer. By assuming that both catenary sections have a near unitary power factor (since modern locomotives are normally driven by bidirectional PWM converters, approximately, at the substation, the power factor could be considered unitary) and by considering sinusoidal current waveforms at the catenary sections, the fundamental currents of both catenary sections x and y are in phase with the overhead catenary voltages $\dot{U}_x$, and $\dot{U}_y$, and are expressed by:

$$\begin{aligned} \dot{I}_{Lx} &= I_{Lx}\, e^{-j30^\circ} \\ \dot{I}_{Ly} &= I_{Ly}\, e^{-j90^\circ} \end{aligned} \tag{3}$$

where, I_{Lx}, I_{Ly} denote the fundamental RMS currents of both catenary sections x, and y, respectively. The three-phase power grid currents in this case are as in Equation (4) and they have the phasors diagram presented in Figure 2a.

$$\begin{aligned} \dot{I}_A &= \tfrac{I_{Lx}}{K_V}\, e^{-j30^\circ} \\ \dot{I}_B &= \tfrac{I_{Ly}}{K_V}\, e^{-j90^\circ} \\ \dot{I}_C &= -\tfrac{I_{Lx}}{K_V}\, e^{-j30^\circ} - \tfrac{I_{Ly}}{K_V}\, e^{-j90^\circ} \end{aligned} \tag{4}$$

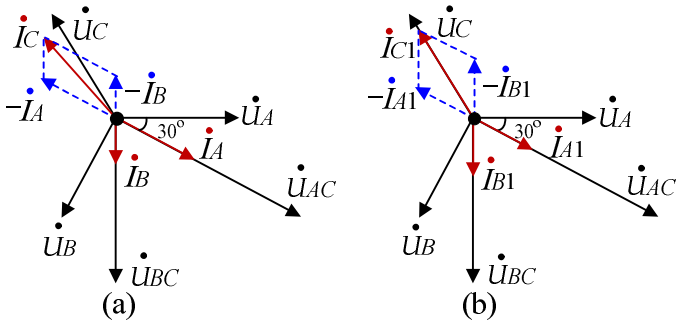

Figure 2. Diagrams of the three-phase power grid currents: (**a**) When both catenary sections are unequally loaded without compensation; (**b**) When balancing the active power between sections.

2.1. Active Power Balancing

The first step to achieving power quality improvement is to balance the active power between sections, considering that the section x load is higher than the section y load. Consequently, phase A current magnitude, which corresponds to section x catenary, will be higher than phase B current magnitude, as shown in Figure 2a. According to Equation (4), phase C current has the highest value in that case. By assuming negligible power losses in the SRPC power switches, SRPC system should shift half of the load currents difference from the heavily to the lightly loaded section, as in Equation (5) [26]. As a result, SRPC system partially contributes to feeding active power required by traction loads. The worst-case scenario for the SRPC to balance active power between sections is when one of the load sections without load (no locomotives supplied by catenary section x or catenary section y) [27].

$$\Delta I = \frac{1}{2}\left(I_{Lx} - I_{Ly}\right) \tag{5}$$

After shifting the active power difference, the three-phase power grid currents are established as in (6). Accordingly and as shown in Figure 2b, phase *A* and phase *B* currents now have the same magnitude, but phase *C* current still has the highest magnitude $\left(I_{C1} = \sqrt{3}\, I_{A1} = \sqrt{3}\, I_{B1}\right)$. However, phase *C* current is in phase with its phase voltage $\dot{U}_C$, while the other two phases currents of $\dot{I}_{A1}$ and $\dot{I}_{B1}$ are shifted 30° angle with the corresponded phase voltages of $\dot{U}_A$ and $\dot{U}_B$, since the reactive power is not yet compensated [26,27].

$$\begin{aligned} \dot{I}_{A1} &= \dot{I}_A - \tfrac{\Delta I}{K_V}\, e^{-j30^\circ} = \tfrac{1}{2K_V}(I_{Lx} + I_{Ly})\, e^{-j30^\circ} \\ \dot{I}_{B1} &= \dot{I}_B + \tfrac{\Delta I}{K_V}\, e^{-j90^\circ} = \tfrac{1}{2K_V}(I_{Lx} + I_{Ly})\, e^{-j90^\circ} \\ \dot{I}_{C1} &= -\dot{I}_{A1} - \dot{I}_{B1} \end{aligned} \tag{6}$$

2.2. Reactive Power Compensation

It is important to add a certain reactive current to phase *x*, and phase *y*, in order to make the three-phase currents balanced without NSC of currents. In this context, section *x* converter compensates a capacitive reactive power and section *y* converter compensates an inductive reactive power when V/V connection is implemented [6]. As presented in Equation (7), the reactive current components have the same RMS value.

$$\begin{aligned} I_{rxr} &= I_{x1} \tan\tfrac{\pi}{6} = \tfrac{1}{2}\,(I_{Lx} + I_{Ly})\, \tan\tfrac{\pi}{6} \\ I_{ryr} &= I_{y1} \tan\tfrac{\pi}{6} = \tfrac{1}{2}\,(I_{Lx} + I_{Ly})\, \tan\tfrac{\pi}{6} \end{aligned} \tag{7}$$

The three-phase power grid currents after active and reactive power compensation have an equal magnitude as presented in Figure 3a. Accordingly, the currents at the secondary side of the V/V power transformer also have equal magnitudes as presented in Equation (8) and Figure 3b. After compensation, the instantaneous waveforms of the phase *x* and phase *y* currents are as in Equation (9).

$$\begin{aligned} \dot{I}_{x2} &= \dot{I}_{x1} + \dot{I}_{rxr} = \tfrac{1}{\sqrt{3}}\,(I_{Lx} + I_{Ly})\, e^{\,j0^\circ} \\ \dot{I}_{y2} &= \dot{I}_{y1} + \dot{I}_{ryr} = \tfrac{1}{\sqrt{3}}\,(I_{Lx} + I_{Ly})\, e^{\,-j120^\circ} \\ \dot{I}_{z2} &= \dot{I}_{x2} + \dot{I}_{y2} = \tfrac{1}{\sqrt{3}}\,(I_{Lx} + I_{Ly})\, e^{\,j120^\circ} \end{aligned} \tag{8}$$

$$\begin{aligned} i_{x2} &= \sqrt{\tfrac{2}{3}}\,(I_{Lx} + I_{Ly})\, \sin(\omega t + 0) \\ i_{y2} &= \sqrt{\tfrac{2}{3}}\,(I_{Lx} + I_{Ly})\, \sin\left(\omega t - \tfrac{2\pi}{3}\right) \end{aligned} \tag{9}$$

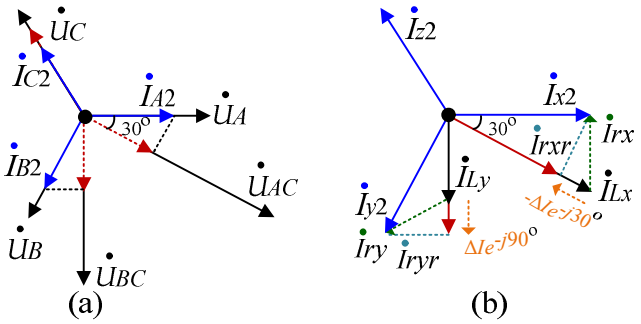

Figure 3. Diagrams of the three-phase power grid currents: (**a**) When both catenary sections are unequally loaded and without compensation; (**b**) When the active power is balanced between sections.

The total compensation currents injected by the SRPC can be obtained from Figure 3b and Equation (10). The positive direction of the compensation current is when it flows into the SRPC as clarified in Figure 1.

$$\begin{aligned} i_{rx}{}^{*} &= i_{x2} - i_{Lx} \\ i_{ry}{}^{*} &= i_{y2} - i_{Ly} \end{aligned} \tag{10}$$

3. SRPC Mathematical Analysis

3.1. Circulating Current Analysis

The MMC circulating currents are produced due to the inner DC-voltage differences between MMC SMs, then, Figure 4 shows the equivalent circuit of one of the MMC phases. As shown, the compensation current of phase x, which should be injected by the SRPC, i_{rx}, consists of two main components: the upper arm current, i_{rxu}, and the lower arm current, i_{rxl}. As presented in Equation (11), the upper arm current, i_{rxu}, includes two main components: the circulating current component, i_{cirx}, and the current related to the compensation current, $i_{rx}/2$. The circulating current flows through the whole MMC phase leg, circulates between the two dc-buses or/and among the MMC legs.

$$i_{rxu} = i_{cirx} - \frac{i_{rx}}{2} \tag{11}$$

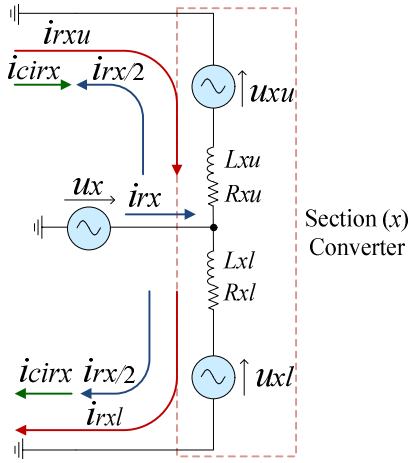

Figure 4. Equivalent circuit of one MMC leg of the SRPC system.

As presented in Equation (12), the lower arm current, i_{rxl}, also includes two main components: the circulating current component, i_{cirx}, and the current related to the compensation current, $i_{rx}/2$.

$$i_{rxl} = i_{cirx} + \frac{i_{rx}}{2} \tag{12}$$

From Equations (11) and (12), the circulating current that flows through the MMC legs can be expressed as in (13), which is composed by two main parts: the double fundamental frequency component of 100 Hz and its even order harmonic contents and a direct current (DC) component results from the DC-link currents [13].

$$i_{cirx} = \frac{i_{rxu} + i_{rxl}}{2} \tag{13}$$

By applying the Kirchhoff's voltage law on the equivalent circuit of Figure 4, it is possible to obtain the voltage equation of the upper and the lower loops as in Equation (14).

$$\begin{aligned} u_x &= -L_{xu}\frac{di_{rxu}}{dt} - u_{xu} - i_{rxu}\,R_{xu} \\ u_x &= L_{xl}\,\frac{di_{rxl}}{dt} + u_{xl} + i_{rxl}\,R_{xl} \end{aligned} \tag{14}$$

3.2. Deadbeat Predictive Current Control

Unlike the PI and PR controllers that compile integral errors, deadbeat predictive control is a technique that attempts to extract the required control action during each sample interval through calculations based on the circuit model of the system being controlled. The accuracy of the equivalent circuit is a significant factor to maintain the system output values equal to the reference signals [25].

Deadbeat predictive current control methodology can be easily programmed, and it is used when a fast-dynamic response is required. However, this control has some disadvantages in terms of existing errors due to the model assumptions and the unmodeled delay introduced by calculation time and modulation [25]. In this context, according to [28], the current control strategies with the smallest tracking error were the synchronous PI, the feedforward in [29], the sliding mode in [30], and the deadbeat predictive control proposed in [31]. Therefore, reference equations based on the deadbeat predictive control in [31] have been extracted in this paper using a low computational cost after neglecting the semiconductor conduction and switching losses. This current control strategy was selected since the results in [31] have a small steady-state error and a fast transient response.

Further steps are applied for the upper arm of section x converter. The deadbeat predictive current control methodology used in this paper can be defined after knowing the error current of the upper arm of section x converter as in (15).

$$i_{rxu\_err} = i^*_{rxu} - i_{rxu} \tag{15}$$

Due to the low-voltage drops across the internal resistors of the MMC arm inductors, the voltage drop across the MMC arm resistors is neglected to simplify the calculations, without introducing significant error. By substituting the first Equation of (14) in (15):

$$u_x = -L_{xu}\frac{d(i^*_{rxu} - i_{rxu\_err})}{dt} - u_{xu} \tag{16}$$

By separating the differential part of Equation (16), the upper arm voltage of section x converter can be presented as in Equation (17).

$$u_{xu} = -L_{xu}\frac{d\,i^*_{rxu}}{dt} + L_{xu}\frac{d\,i_{rxu\_err}}{dt} - u_x \tag{17}$$

It is feasible to assume a linear variation of $i_{rxu\_err}(k)$ with the time, where (k) denotes the value at the present sample interval and the next sample interval is denoted as $(k+1)$. According to Equation (18), an assumption of $i^*_{rxu}(k)$ derivative in function to the variables value is possible at the instant of (k) and $(k-1)$. Then, it is feasible to get Equation (19), where T_s refers to the sampling period.

$$\frac{dx}{dt} \cong \frac{x\,(k) - x\,(k-1)}{T_s} \tag{18}$$

$$u_{xu}(k) = -\frac{L_{xu}}{T_s}[\,i^*_{rxu}\,(k) - i^*_{rxu}(k\ -1) - i_{rxu\_err}(k)] - u_x(k) \tag{19}$$

By substituting Equation (15) in (19):

$$u_{xu}(k) = \frac{L_{xu}}{T_s}[-2\,i^*_{rxu}\,(k) + i^*_{rxu}(k-1)\ + i_{rxu}(k)] - u_x(k) \tag{20}$$

The SRPC control algorithm should calculate the compensation current references, i^*_{rx}, and i^*_{ry}, as in Equation (10), respectively. Therefore, Equation (20) as it is does not serve that purpose, since it computes the compensation current references of the upper and the lower MMC arms, i^*_{rxu}, and i^*_{ryu}. The main purpose of this control is to have a near zero circulating current, i_{cirx}, and i_{ciry}, in the MMC phases, then from Equation (13), the circulating current is significantly reduced when the upper and the lower arm currents are complementary as in Equation (21).

$$i_{cirx} = \frac{i_{rxu} + i_{rxl}}{2} \cong 0 \Rightarrow i_{rxu} \cong - i_{rxl} \tag{21}$$

By considering the aforementioned assumptions:

$$\begin{array}{l} i_{rxu} = -\frac{i_{rx}}{2} \\ i_{rxl} = +\frac{i_{rx}}{2} \end{array} \tag{22}$$

By substituting Equation (22) in (20), the equation that calculates the upper arm voltage, u_{xu}, in relation with the phase x compensation current reference, i^*_{rx}, is presented as Equation (23).

$$u^*_{xu}(k) = \frac{L_{xu}}{2T_s}\left[2i^*_{rx}(k) - i^*_{rx}(k-1) + 2i_{rxu}(k)\right] - u_x(k) \tag{23}$$

The same previous steps are applicable to conclude the voltage reference final equation for the lower MMC arm of section x as presented in (24).

$$u^*_{xl}(k) = -\frac{L_{xl}}{2T_s}\left[2i^*_{rx}(k) - i^*_{rx}(k-1) - 2i_{rxl}(k)\right] + u_x(k) \tag{24}$$

The voltage reference final equations for the upper and the lower MMC arms of section y are presented in (25) and (26). Equations (23)–(26) are the final voltage reference equations to apply the deadbeat predictive control, considering the suppression of the MMC circulating currents. Then, these voltages (average voltages during a switching cycle) are applied using a modulator to drive the power semiconductor switches.

$$u^*_{yu}(k) = \frac{L_{yu}}{2T_s}\left[2i^*_{ry}(k) - i^*_{ry}(k-1) + 2i_{ryu}(k)\right] - u_y(k) \tag{25}$$

$$u^*_{yl}(k) = -\frac{L_{yl}}{2T_s}\left[2i^*_{ry}(k) - i^*_{ry}(k-1) - 2i_{ryl}(k)\right] + u_y(k) \tag{26}$$

4. SRPC Control Algorithm

4.1. Establishing the Compensation Current References

The compensation currents in (10) can be implemented by using the instantaneous load section currents as in Equations (27) and (28), where, I_{Lxa}, and I_{Lya}, are the RMS active currents of the load sections. The current components of I_{Lxr}, and I_{Lyr}, are the RMS reactive currents of the load sections. The components of I_{Lxh}, and I_{Lyh}, are the h^{th} order harmonic contents for both load sections, then, $\varnothing_{xh}$ *and* $\varnothing_{yh}$ are the corresponding phase angles of the h^{th} order harmonic current [26,32].

$$i_{Lx} = \sqrt{2}\, I_{Lxa} \sin\left(\omega t - \frac{\pi}{6}\right) + \sqrt{2}\, I_{Lxr} \sin\left(\omega t - \frac{2\pi}{3}\right) + \sum_{h=2}^{\infty} \sqrt{2}\, I_{Lxh} \sin(h\omega t + \varnothing_{xh}) \tag{27}$$

$$i_{Ly} = \sqrt{2}\, I_{Lya} \sin\left(\omega t - \frac{\pi}{2}\right) + \sqrt{2}\, I_{Lyr} \sin(\omega t - \pi) + \sum_{h=2}^{\infty} \sqrt{2}\, I_{Lyh} \sin\left(h\omega t + \varnothing_{yh}\right) \tag{28}$$

Multiplying Equation (27) by $\sin(\omega t - \pi/6)$ gives a DC current component of $\sqrt{2}/2\, I_{Lxa}$, as presented in Equation (29).

$$i_{Lx}\sin\left(\omega t - \tfrac{\pi}{6}\right) = \tfrac{\sqrt{2}}{2} I_{Lxa} - \tfrac{\sqrt{2}}{2} I_{Lxa}\cos\left(2\omega t - \tfrac{\pi}{3}\right) - \tfrac{\sqrt{2}}{2} I_{Lxr}\cos\left(2\omega t - \tfrac{5\pi}{6}\right) + \sum_{h=2}^{\infty} \sqrt{2}\, I_{Lxh}\sin(h\omega t + \varnothing_{xh})\sin\left(\omega t - \tfrac{\pi}{6}\right) \quad (29)$$

In a similar way, by multiplying Equation (28) by $\sin(\omega t - \pi/2)$, this results in a DC current component of $\sqrt{2}/2\, I_{Lya}$. Summing the DC components of $\sqrt{2}/2\, I_{Lxa}$, and $\sqrt{2}/2\, I_{Lya}$, then multiplying the result with the value of $2/\sqrt{3}$ gives the peak value of phase x current after compensation $I_{x2m} = \sqrt{2/3}\,(I_{Lx} + I_{Ly})$ (taking into consideration that load power factor is close to unitary). Extracting the DC current component of $\sqrt{2/3}\,(I_{Lx} + I_{Ly})$ is possible after using a digital moving average low pass filter (LPF).

On the other hand, using two single-phase enhanced phase-locked loop (E-PLL) is essential to acquire the phase angles for both catenary voltages of u_x, and u_y. The E-PLL generates an output waveform whose phase is related to the phase of an input waveform. It also generates an output waveform that lags the input waveform by 90 degrees [33]. In this case, the instantaneous currents of phase x and phase y after compensation are generated. Then, using Equation (10) gives the compensation current references. The next step is to use a controller to track these reference currents, as explained in the next paragraph Figure 5 shows the block diagram for establishing the references of compensation currents.

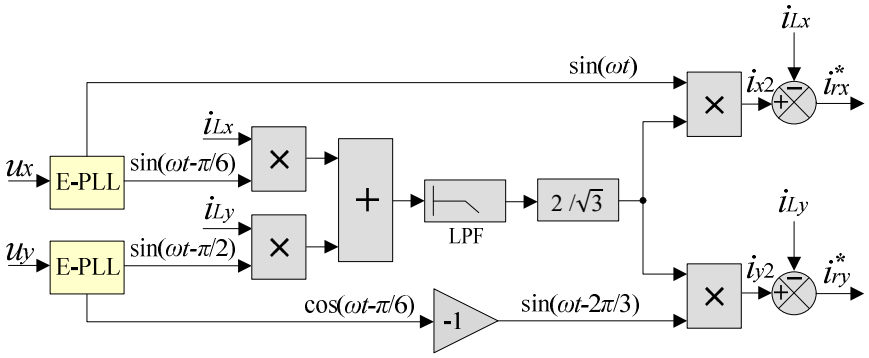

Figure 5. Diagram for establishing the references of compensation currents. E-PLL: definition.

4.2. DC-Bus Voltage Balancing and Tracking of the Reference Signals

Hereafter, the symbol σ refers to both catenary sections of x and y. The symbols l, u denote the lower and the upper MMC arms, respectively. Two PI controllers are responsible to achieve the voltage balancing control for the MMC main DC-link voltage as shown in the control strategy of Figure 6a. The first PI controller is used to compare the actual value of the DC-link voltage with its reference value V^*_{dc}. The output of this PI controller is multiplied by two synchronizing signals to obtain the dc-link voltage regulation signals of section x and section y converters. The second PI controller balances the voltages between the two DC-link capacitors. The output signal of this controller is added to the compensation current references, $i_{rx}{}^*$, and $i_{ry}{}^*$. Equations (23)–(26) are implemented in the digital controller to implement the deadbeat predictive current control methodology for circulating currents reduction in the MMC (the source code to implement the Equations (23)–(26) in the controller is shown in the Appendix A). This leads to generate the upper and the lower voltage reference signals for each MMC arm.

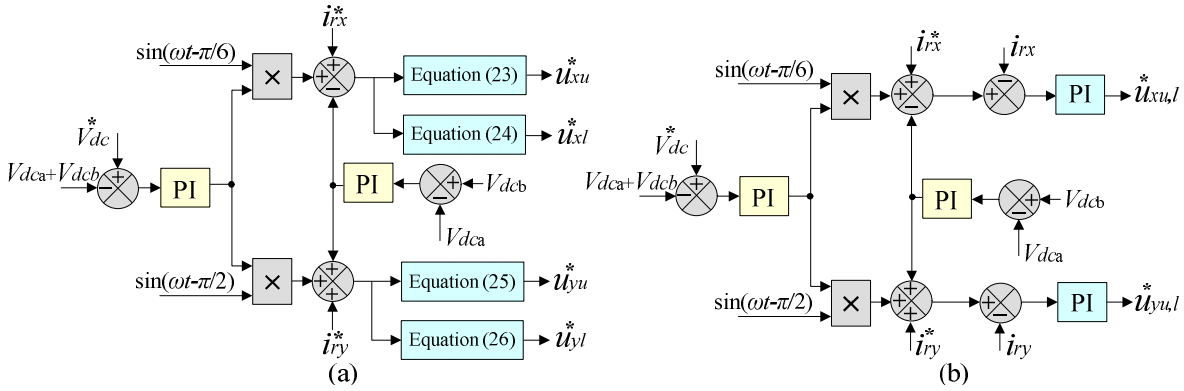

Figure 6. Voltage control and calculation of the voltage reference signals: (**a**) When using the deadbeat predictive control; (**b**) When using the conventional PI control.

On the other hand, and since one of the contributions of this paper is to establish a comparison between the deadbeat predictive current control methodology and the conventional PI controller, Figure 6b shows the DC-link voltage control and the calculation of the voltage reference signals when using the conventional PI controller. It is noteworthy to mention that conventional stationary frame PI controllers are not practically favorable to serve this application, since they cannot reach the zero steady-state error, but they are good enough for the demonstration.

4.3. SM Voltages Balancing Control

Figure 7a shows an averaging voltage balancing control for the SM capacitors. This control ensures that the voltage of each SM in the leg is close to the average voltage that is provided as a reference. It is implemented by summing the measured SM voltages for each MMC leg and dividing the result by the number of SMs per leg. The actual average voltage value, in this case, is calculated and compared to a reference average voltage, V^*_{SM}. Then, a PI controller is used to correct the difference between the actual and the reference values [6,32]. The output of this controller is considered as a reference for a circulating current controller, which it is implemented by summing the upper and the lower arm currents for each converter as in (21). This controller allows a low circulating current when it is necessary to balance the SM voltages.

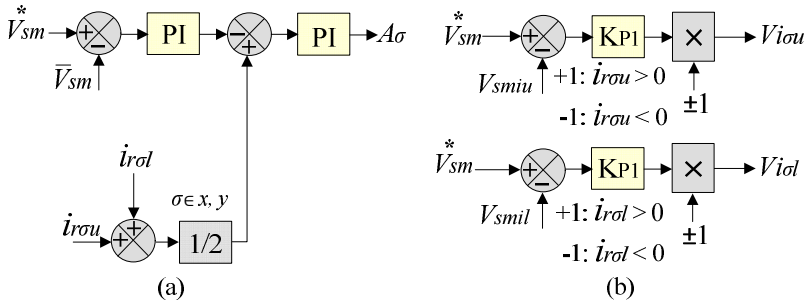

Figure 7. Voltages balancing control: (**a**) Averaging voltage balancing control; (**b**) Individual voltage balancing control.

The individual voltage balancing control presented in Figure 7b forces the capacitor voltage of each SM to follow its reference, which is performed by a proportional controller for each SM to act dynamically in the balancing process in every switching period [6]. The output of the individual voltage balancing controller is multiplied by +1 if the arm's current direction is to charge the capacitors, or by –1 if its direction is to discharge the capacitors (the positive directions of MMC arm currents are presented in Figure 1).

Figure 8 shows the voltage command generation for the two-level SM applied to a phase-shifted PWM. The final averaging voltage control signals of A_σ, the final individual voltage control signals of $V_{i\sigma}(l,u)$, were added to the obtained final reference waveforms of $u_\sigma{}^*(l,u)$. By taking into consideration twenty-four SMs in each MMC leg, so the total SMs number will be divided equally between the upper and the lower arms in the same phase leg, then the arm will consist of twelve SMs (N = 13, Thirteen-levels MMC). Consequently, the phase-shifted PWM triangular carriers in one MMC arm are shifted 360/12 = 30° between each other.

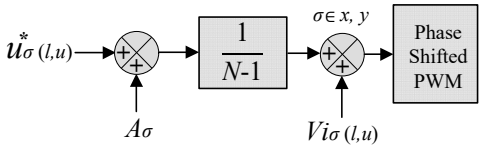

Figure 8. Command generation for each two-level SM applied to a phase-shifted PWM.

5. Simulation Results

An MMC with a few levels is sufficient for a proof-of-concept of the deadbeat predictive current control, then, the simulation model of the SRPC consists of twenty-four SMs per each leg (13-levels), and it was developed under *PSIM* v9.1 simulation tool, where the main parameters are presented in Tables 1 and 2. The main objective is to perform a comparative study when using the deadbeat predictive control for circulating current reduction in MMC (presented in Figure 6a), and when using the conventional PI controller (presented in Figure 6b) to track the reference signals of $i_{rx}{}^*$, and $i_{ry}{}^*$. In addition, and in order to show the advantages of the presented deadbeat predictive current control methodology, simulation results are presented under transient load conditions.

Table 1. Simulation model parameters.

Parameter	Symbol	Value
Power grid voltage	U_{AB}	110 kV
Traction grid voltage	$U_\sigma;\ \sigma \in \{x, y\}$	25 kV
Fundamental frequency	f	50 Hz
Section x load power	P_{Lx}	1.75 MW
Section y load power	P_{Ly}	2.62 MW
V/V transformer turns ratio	K_V	110:25

Table 2. MMC parameters applied to simulation model.

Parameter	Symbol	Value
Number of SM per MMC arm	N-1	12
DC-link voltage	$V_{dc} = V_{dca} + V_{dcb}$	72 kV
Single SM voltage	V_{SM}	6 kV
Switching frequency of each SM	f_{isw}	3 kHz
Equivalent switching frequency	f_{sw}	36 kHz
MMC arm inductor	$L_{\sigma(u,l)};\ \sigma \in \{x, y\}$	3 mH
SM capacitance	C_{SM}	900 µF
DC-bus capacitance	$C_{dca} = C_{dcb}$	5 mF

The value of the MMC arm inductor directly influences the control system in terms of capability to track the compensation current references. As the current ripples depend on the voltage applied on the MMC arm inductor, the value of the inductor and the time that the voltage is applied, the MMC arm inductor can be designed by considering the factors of current ripples suppression, and the speed of signal tracking. A low value of capacitance in the SM implies high voltage ripples. However, a high value of capacitance implies costly and bulky MMC. In this context, the previous aspects were

considered in the selection process of the SM capacitance and the MMC arm inductors, where the values presented in Table 2 were selected based on a trade-off between the size, cost, current ripples and voltage ripples.

Since the power factor of the electric locomotives in high-speed trains is close to unitary and the current harmonics are quite small [26], the high-speed railway electric locomotive is modeled as a resistive-inductive load in parallel with an uncontrollable rectifier bridge connected to the secondary side of the locomotive transformer, as shown in Figure 9 [26]. The output of the uncontrollable rectifier bridge is connected to resistor R_2 and inductor L_2, which are in series. The turns ratio of the locomotive transformer is 25:1.5. The locomotive model parameters are selected as $R_1 = 2\ \Omega$, $R_2 = 3.3\ \Omega$ and $L_2 = 0.8$ mH. At these values, section x load power is near 1.75 MW. Section y load power is chosen to be 150% higher than section x load power, as presented in Table 1.

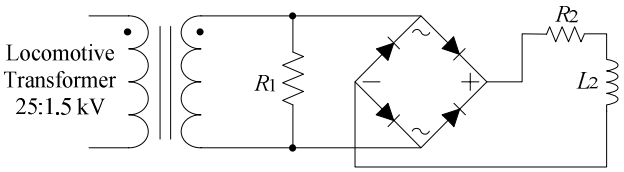

Figure 9. Model used in simulation.

This case study presents the results for two scenarios: (a) When using the deadbeat predictive current control methodology; (b) When replacing the Equations (23)–(26) in Figure 6a by conventional PI controllers, as shown in Figure 6b, to correct the error signals of $i^*_{rx} - i_{rx}$ and $i^*_{ry} - i_{ry}$, as explained in [6]. The results for both cases are presented after considering the same control parameters (similar PI parameters) of the MMC DC-link voltage presented in Figure 6, averaging voltage balancing control (for each MMC leg) presented in Figure 7a, and the individual voltage balancing control (for each SM) presented in Figure 7b.

Figure 10a shows the three-phase currents before compensation. The currents are imbalanced and have NSC of currents. On the other hand, Figure 10b presents the same currents after the SRPC compensates reactive power and shifts half of the active power difference between catenary sections. At that case, the three-phase currents are balanced and sinusoidal. The catenary section currents of i_{Lx} and i_{Ly} at unitary load power factor are presented in Figure 10c. It is important to note that the results presented in Figure 10 are very similar when using the deadbeat predictive control or the PI controllers. The three-phase currents before compensation, i_A, i_B, and i_C, and the catenary section currents, i_{Lx}, and i_{Ly}, have no relation with the SRPC system operation. The three-phase currents after compensation, i_{A2}, i_{B2}, and i_{C2}, are resulting after injecting the compensation currents of i_{rx}, and i_{ry}. The compensation currents are calculated according to the catenary section currents of i_{Lx}, and i_{Ly}, as in (10). In addition to that, and as has mentioned before, the circulating currents do not contribute to the compensation currents injected by the SRPC system. Therefore, the three-phase currents after compensation should have almost similar waveforms regardless of the controller used.

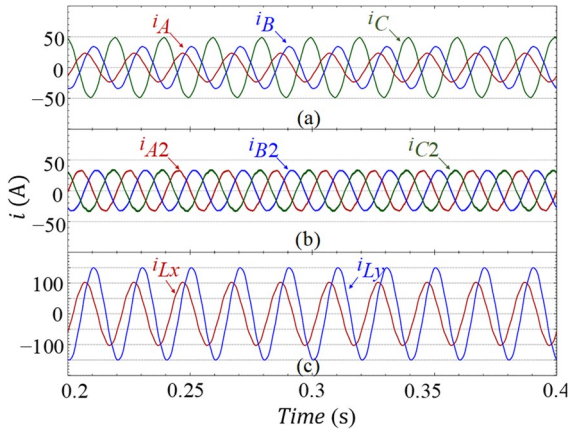

Figure 10. Simulation results: (**a**) Three-phase grid currents before compensation; (**b**) Three-phase grid currents after compensation; (**c**) Catenary section (x and y) currents.

Figure 11A presents the results when using the deadbeat predictive current control methodology for circulating current suppression. Figure 11A(a) presents the SRPC compensation currents. Phase x compensation current, i_{rx}, has a higher value than in phase y, i_{ry}, because catenary section y has a higher load value, as referred in Table 1. Figure 11A(b,c) shows the MMC arm currents. Note that subtracting the lower arm current, $i_{r\sigma l}$, from the upper arm current, $i_{r\sigma u}$, gives the MMC compensation current, $i_{r\sigma}$. Figure 11A(d) shows the circulating currents in the MMC legs, $i_{cir\sigma}$. The circulating currents were calculated according to Equation (13) and they have an average value of 5 A. This small current component is important to accomplish the balance between the MMC SM voltages.

Figure 11B(a) presents the simulation results when using well-tuned conventional PI controllers, as shown in Figure 6b. The compensation currents injected into the power grid presented in Figure 11A(a) and Figure 11B(a) are similar, and have no relation with the MMC circulating currents. However, the upper and the lower arm currents presented in Figure 11B(b,c) are quite different from the ones presented in Figure 11A(b,c). In this case, arm currents have higher harmonic contents and higher RMS value due to the circulating currents between the MMC legs, which have an RMS value of 9.8 A, as shown in Figure 11B(d). As a result, the circulating current component distorts the MMC arm currents.

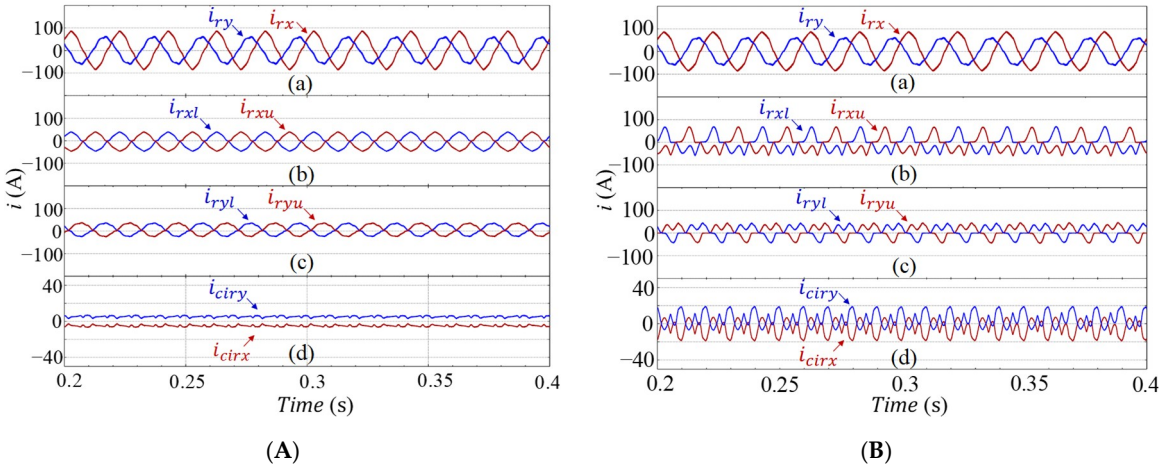

Figure 11. Currents when using the predictive current controller (**A**) and when using the conventional PI controllers (**B**): (**a**) SRPC compensation currents; (**b**) Upper and lower arm currents of section x converter; (**c**) Upper and lower arm currents of section y converter; (**d**) MMC circulating currents.

The frequency spectrum of SRPC compensation currents when using the deadbeat predictive current control methodology for circulating current suppression is presented in Figure 12A(a,b), where only fundamental current components of 50 Hz are present. In that case, the circulating currents frequency spectrum presented in Figure 12A(c,d) mainly shows DC components, which are important for the SM voltage balancing control, besides regulating the main DC-link voltage. On the other hand, Figure 12B(a,b) shows the frequency spectrum of SRPC compensation currents when using well-tuned conventional PI controllers. The circulating currents do not contribute to the total compensation currents. Therefore, the frequency spectrum of SRPC compensation currents presented in Figure 12A(a,b) is similar to the one presented in Figure 12B(a,b). The circulating currents in this case have the multiples of the second-order frequency component (100 Hz), as shown in Figure 12B(c,d).

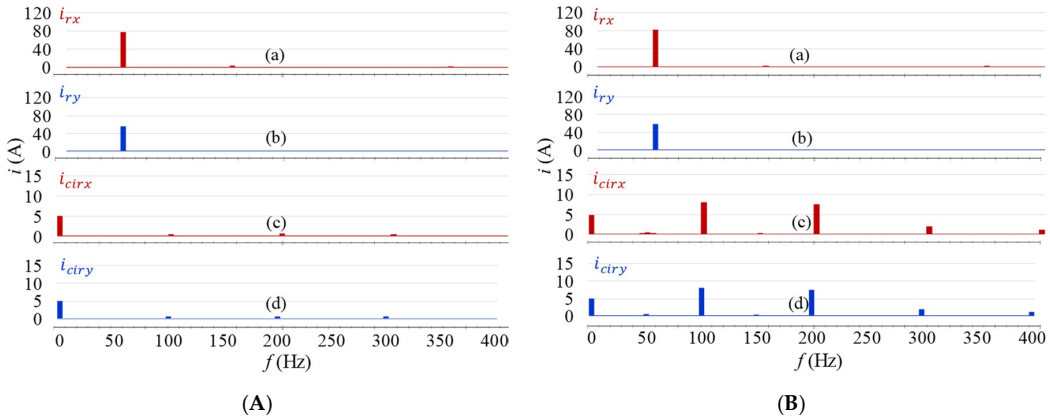

Figure 12. Spectrum of currents when using the predictive current controller (**A**) and when using the conventional PI controllers (**B**): (**a**) Compensation current of section *x* converter; (**b**) Compensation current of section *y* converter; (**c**) Circulating current of section *x* converter; (**d**) Circulating current of section *y* converter.

Figure 13A(a–d) shows the frequency spectrum of the MMC arm currents when using the deadbeat predictive current control methodology for circulating current suppression. There are no second-order components (100 Hz and other even-order harmonics, such as 4th, 6th, and 8th) in the MMC arm currents, which proves the effectiveness of the deadbeat predictive control methodology for circulating current suppression. This methodology mainly eliminates the even-order harmonics of the circulating currents, but it does not eliminate the DC component of the circulating currents, which is important to achieve the SM voltage balancing control. On the other hand, and due to the fact that circulating current harmonics exist when using the conventional PI controllers, the frequency spectrum of the MMC upper and lower arm currents, in this case, shows the orders of the even-order harmonics. This is shown in Figure 13B(a–d).

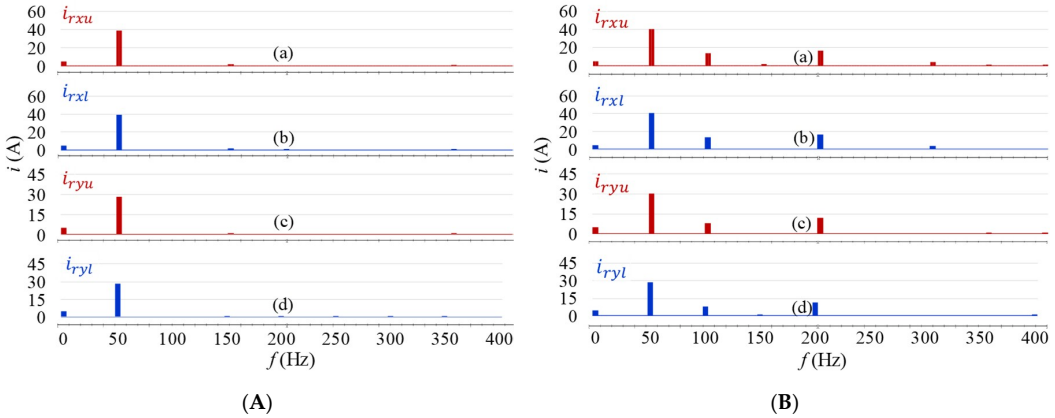

Figure 13. Spectrum of currents when using the predictive current controller (**A**) and when using the conventional PI controllers (**B**): (**a**) Upper arm current of section *x* converter; (**b**) Lower arm current of section *x* converter; (**c**) Upper arm current of section *y* converter; (**d**) lower arm current of section *y* converter.

Figure 14A shows the MMC DC-voltages when using the deadbeat predictive current control methodology: the DC-link voltages are presented in Figure 14A(a), the SM voltages of section *x* converter ($v_{SMx,up}$: for the upper arm SM voltages, $v_{SMx,low}$: for the lower arm SM voltages) and section *y* converter ($v_{SMy,up}$: for the upper arm SM voltages, $v_{SMy,low}$: for the lower arm SM voltages) are presented in Figure 14A(b,c), respectively. Figure 14B shows the MMC DC-voltages when using the PI controllers and when there are circulating currents in the MMC arms: the DC-link capacitor voltages in Figure 14B(a), the SM voltages of section *x* converter ($v_{SMx,up}$: for the upper arm SM voltages, $v_{SMx,low}$: for the lower arm SM voltages), and the SM voltages of section *y* converter ($v_{SMy,up}$: for the upper arm SM voltages, $v_{SMy,low}$: for the lower arm SM voltages) in Figure 14B(b,c), respectively. These waveforms confirm the effectiveness of the voltage balancing control algorithm presented in Figures 6 and 7.

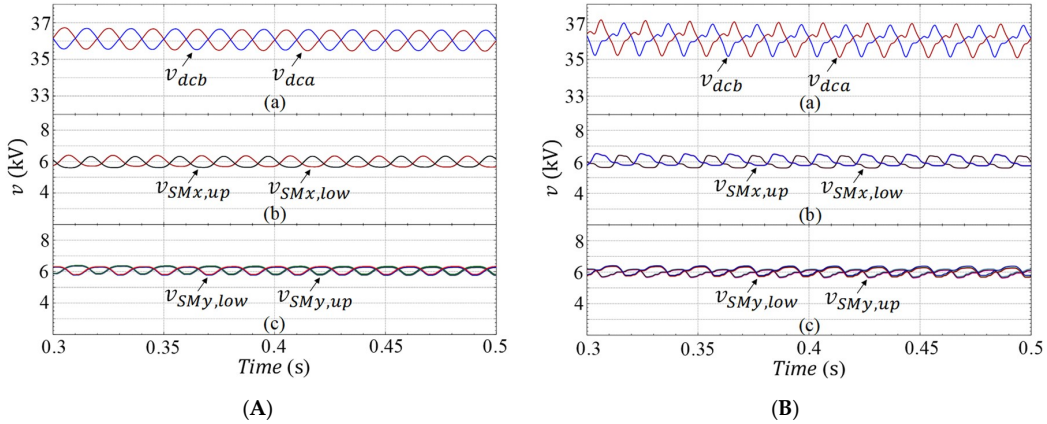

Figure 14. DC-voltages when using the predictive current controller (**A**) and when using the conventional PI controllers (**B**): (**a**) DC-link capacitors voltage; (**b**) SM voltages of section *x* converter; (**c**) SM voltages of section *y* converter.

Besides the operation in steady-state, simulation results showing the SRPC system performance in transient conditions were also obtained. A variable load power was adopted to study the dynamic response of the SRPC system when using the deadbeat predictive current controller. For this purpose, Table 3 presents the load section power values during the simulation. The results do not show the instants between 0 and 0.4 s, since the SRPC converter does not reach the steady-state operation before the 0.4 s. Between the instants 0.4 s and 0.6 s, load section *x* and section *y* have the loads of 1.75 MW

and 2.62 MW, respectively. However, double these power values is applied between 0.6 s to 0.8 s. After 0.8 s, both load sections have the same power of 5.24 MW.

Table 3. Section power values during the simulation.

Time	0.4 s to 0.6 s	0.6 s to 0.8 s	0.8 s to 1.0 s
Section x power	1.75 MW	3.5 MW	5.24 MW
Section y power	2.62 MW	5.24 MW	5.24 MW

Figure 15 shows the SRPC simulation results in transient conditions. The three-phase currents before compensation are shown in Figure 15a. As shown in this case, the three-phase currents are imbalanced and have NSC of currents. The imbalance ratio (ratio of the NSC of currents) is the smallest between 0.8 s and 1.0 s since both load sections have the same power of 5.24 MW. Figure 15b shows the three-phase currents after compensating reactive power and shifting the active power between sections. The currents are balanced and the SRPC system can follow the dynamic changes of the loads. Figure 15c shows the catenary load section currents of i_{Lx} and i_{Ly}. Between 0.4 s and 0.8 s, the load section y has always the double of the load value of the load section x. However, after 0.8 s, both load sections have the same loading parameters.

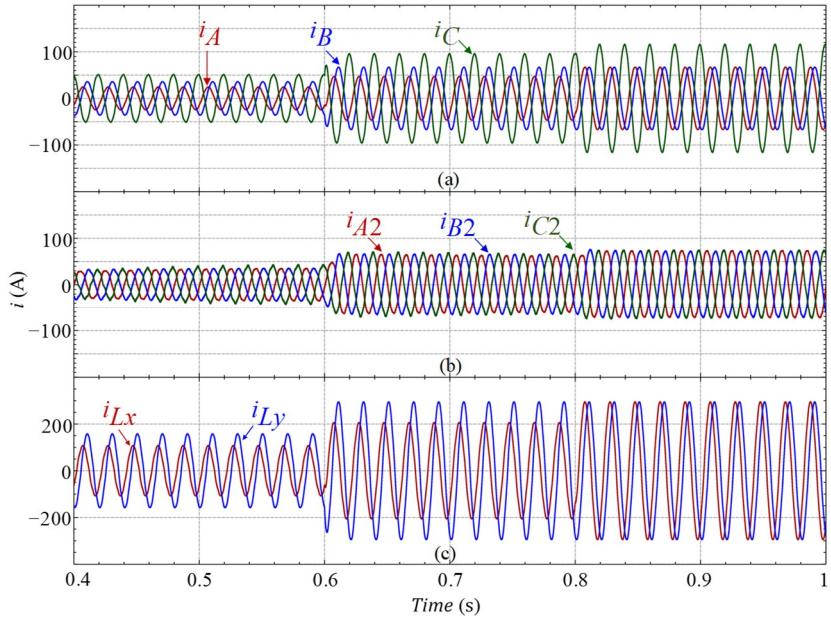

Figure 15. Simulation results under load transients: (**a**) Three-phase grid currents before compensation; (**b**) Three-phase grid currents after compensation; (**c**) Catenary section (x and y) currents.

Figure 16 shows the MMC currents when using the predictive current controller under load dynamic changes. The compensation currents value of i_{rx}, and i_{ry} changes dynamically according to the loading conditions of the load sections, as shown in Figure 16a. It is worthy to mention that, from 0.6 s to 0.8 s, the compensation currents synthesized by the SRPC system are higher than in the case between 0.4 s and 0.6 s. This is because the power difference between the load sections is higher from 0.6 s to 0.8 s. Figure 16b,c shows the upper and the lower arm currents of the section x and section y converter, respectively. Note that subtracting the lower arm current from the upper arm current gives the MMC compensation current. The arm currents have mainly the fundamental frequency component of 50 Hz and a DC current component (the circulating current), which is important to achieve the voltage balance control of the MMC. Figure 16d shows the circulating currents, i_{cirx}, and i_{ciry}, where these currents do not contribute to the compensation currents injected by the SRPC. The higher the

load power difference between the load sections, the higher the circulating current component in the MMC. At high load power difference, the MMC should inject a higher amount of power to compensate the reactive power and shift the active power difference between the sections. This entails to higher circulating current to balance the MMC DC-links (the MMC main DC-link and the SM DC-links) since a higher energy is provided by the converter.

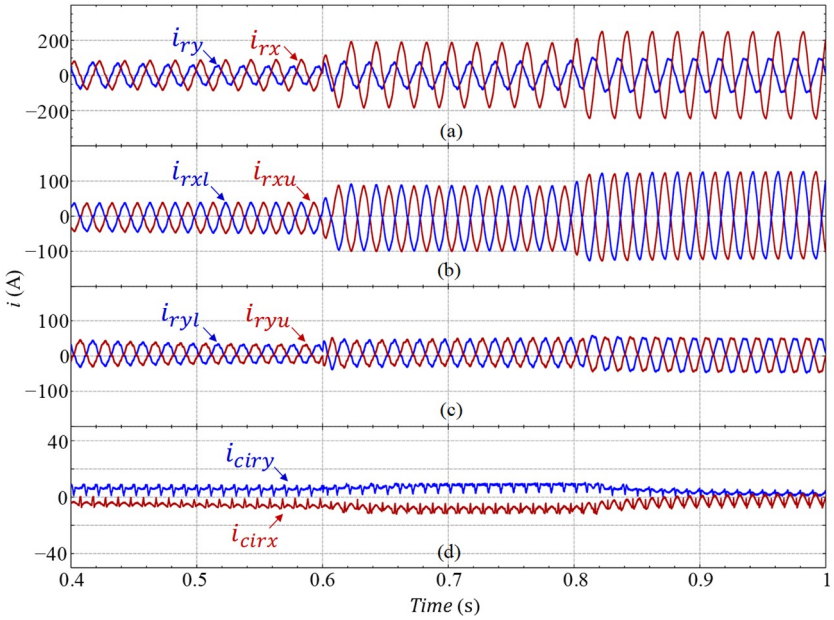

Figure 16. Currents when using the predictive current controller under load transients: (**a**) SRPC compensation currents; (**b**) Upper and lower arm currents of section *x* converter; (**c**) Upper and lower arm currents of section *y* converter; (**d**) MMC circulating currents.

A high value of the circulating currents increases the amplitude of the DC-voltages ripple, hence, the DC-link voltages waveform of Figure 14A(a) have lower voltage ripples when using the deadbeat predictive current control methodology. On the contrary, Figure 14B(a) shows higher voltage ripples of the DC-link voltages when using the conventional PI controllers. On the other hand, the circulating currents may lead to an easier tuning of the SM voltages balancing control and the main DC-link voltage control. As a result, the overflow/over-suppression of the MMC circulating currents is a trade-off between several factors, such as, higher/lower MMC power losses, higher/lower MMC equipment power ratings, robust/fragile DC-voltages control and higher/lower DC-voltage ripples. Therefore, attention must be considered since the over-suppression of the MMC circulating current may affect the response of the SM voltage balancing control. The advantages of the deadbeat predictive current control methodology for circulating current suppression can be summarized as follows:

1. Removing the AC components of the MMC circulating current, then, the circulating current amplitude is reduced while keeping balanced SM voltages. The DC component of the circulating current is essential to keep the SM voltages of MMC around a reference value.
2. Reducing the RMS value of the MMC arm currents.
3. Reducing the voltage ripples in the SM DC-link capacitor.
4. The suppression of circulating current does not disturb the MMC main functionality (in this study, MMC operated as a power quality compensator for electric railway applications).

On the other hand, as specific aspects of the deadbeat predictive current control methodology applied for circulating current suppression can be summarized as follow:

1. Being a deadbeat-based control methodology, unmodeled errors in the SRPC mathematical model often deteriorate the system performance. These unmodeled errors may lead to make the

calculated voltage references deviate from the expected reference values. However, the one-cycle time delay and arm inductor resistance can be included in a more complex model.

2. The presented control methodology is only valid for fixed switching frequency applications.

6. Conclusions

This paper presented and discussed a deadbeat predictive current control methodology to suppress the circulating currents in a modular multilevel converter (MMC) when operating as a simplified rail power conditioner (SRPC). The presented predictive control methodology has a simple and short computational algorithm regardless of the number of MMC submodule (SM). In other words, the computational algorithm of the deadbeat predictive current control methodology for circulating current suppression does not become more complex when increasing the MMC level or inserting extra SMs. The obtained results show suppressed circulating currents (mainly the even-order harmonics), reduced root mean square (RMS) value of the MMC arm currents, and reduced voltage ripples in the SM DC-link capacitor. The frequency spectrum of the MMC arm currents, in that case, do not show even-order harmonic contents, and it mainly has the fundamental frequency component of 50 Hz. However, the presented predictive control methodology does not suppress the DC component of the MMC circulating current, which is essential to maintain the SM voltages of MMC around a reference value. The suppression of circulating current does not disturb the MMC main functionality as a power quality conditioner. Furthermore, simulation results showed balanced three-phase power grid currents without negative sequence components of currents. To some extent, although the inaccuracies in determining the parameter values of the model may increase the control instability and often deteriorate the system performance, the presented deadbeat predictive control can offer a new attempt for circulating current suppression in MMC, which can expand the research ideas as well.

Author Contributions: M.T. performed the control analysis study, validation of the simulation models, and the writing—original draft preparation. All the authors participated in the conceptualization, methodology, and writing—review and editing. All authors have read and agreed to the published version of the manuscript.

Funding: This work has been supported by the Portuguese Foundation of Science and Technology (FCT), in Portuguese, Fundação para a Ciência e Tecnologia within the R&D Units Project Scope: UIDB/00319/2020 and PTDC/EEI-EEE/28813/2017. The first author Mohamed Tanta is supported by FCT Ph.D. grant with a reference PD/BD/127815/2016.

Conflicts of Interest: The authors declare no conflict of interest.

Nomenclature

A_σ	Output of MMC leg averaging voltage control
C_{dca}, C_{dcb}	Capacitance of the MMC DC-bus capacitors
f	Electrical grid fundamental frequency
f_{isw}	Individual SM switching frequency
f_{sw}	Equivalent switching frequency
i_A, i_B, i_C	Phase A, phase B and phase C instantaneous currents before compensation
I_A, I_B, I_C	Phase A, phase B and phase C RMS currents before compensation
I_{A1}, I_{B1}, I_{C1}	Phase A, phase B and phase C RMS currents after active power balance
I_{A2}, I_{B2}, I_{C2}	Phase A, phase B and phase C RMS currents after active power balance and reactive power compensation
i_x, i_y, i_z	Phase x, phase y and phase z instantaneous currents of the secondary windings of the V/V power transformer before compensation.
I_x, I_y, I_z	Phase x, phase y and phase z RMS currents of the secondary windings of the V/V power transformer before compensation.

I_{x1}, I_{y1}, I_{z1}	Phase x, phase y and phase z instantaneous currents of the secondary windings of the V/V power transformer after active power balance.
I_{x2}, I_{y2}, I_{z2}	Phase x, phase y and phase z instantaneous currents of the secondary windings of the V/V power transformer after active power balance and reactive power compensation.
i_{cirx}, i_{ciry}	MMC instantaneous circulating current
i_{Lx}, i_{Ly}	Load section instantaeous currents
I_{Lx}, I_{Ly}	Load section RMS currents
I_{Lxa}, I_{Lya}	RMS load section active currents
I_{Lxh}, I_{Lyh}	RMS h^{th} order harmonic current contents for both load sections
I_{Lxr}, I_{Lyr}	RMS load section reactive currents
i_{rx}^{*}, i_{ry}^{*}	Instantaemous compensation current references
i_{rx}, i_{ry}	Instantaneous compensation currents synthesized by SRPC system
i_{rx_err}	Instantaneous error current
I_{rxr}, I_{ryr}	Reactive RMS compensation currents synthesized by SRPC
i_{rxu}, i_{rxl}	Instantaneous upper and lower arm currents of MMC section x converter
i_{ryu}, i_{ryl}	Instantaneous upper and lower arm currents of MMC section y converter
K_V	Turns ratio of the V/V power transformer
k	Present sample interval
L_{xu}, L_{xl}	Upper and lower arm inductors of the MMC section x converter
L_{yu}, L_{yl}	Upper and lower arm inductors of the MMC section y converter
N	MMC Voltage Level
N-1	Number of SM in one MMC arm
R_{xu}, R_{xl}	Upper and lower arm equivalent resistance of the MMC section x converter
R_{yu}, R_{yl}	Upper and lower arm equivalent resistance of the MMC section y converter
T_s	Sampling period
U_A, U_B, U_C	Phase-to-line RMS voltages of the three-phase public power grid
U_{AC}, U_{BC}	Line-to-line RMS voltages of the three-phase public power grid
u_x, u_y	Phase x and phase y instantaneous load section voltages
U_x, U_y	Phase x and phase y RMS load section voltages
u_{xu}^{*}, u_{xl}^{*}	Instantaneous reference signals of the upper and the lower MMC arm of section x converter
u_{xu}, u_{xl}	Instantaneous upper and lower MMC arm voltages of section x converter
u_{yu}^{*}, u_{yl}^{*}	Instantaneous reference signals of the upper and the lower MMC arm of section y converter
u_{yu}, u_{ul}	Instantaneous upper and lower MMC arm voltages of section y converter
v_{dca}, v_{dcb}	Instantaneous DC-link voltage of upper and lower arm of section x converter
V_{dc}^{*}	The reference value of the DC-link voltage
V_{sm}^{*}	The reference value of the SM DC-link voltage
V_{smiu}, V_{smil}	The individual SM voltage in the upper and the lower MMC arm, respectively
$V_{i\sigma u}$, $V_{i\sigma l}$	Output of MMC SM individual voltage control
	Average DC-voltage in one MMC leg
$v_{smx,up}$, $v_{smx,low}$	Instantaneous SM voltages of upper and lower arm of section x converter
$v_{smy,up}$, $v_{smy,low}$	Instantaneous SM voltages of upper and lower arm of section y converter
ΔI	Active RMS compensation currents synthesized by RPC
ϕ_{xh}, ϕ_{yh}	The corresponded phase angles of the h^{th} order harmonic current contents for both load sections

Appendix A

```
//source code to implement the deadbeat control Equations (23)–(26) in the controller.
double Iry_ref, Irx_ref;
//Controller input signals (calculated using the Figure 5)
double Irx, Iry, Irxu, Irxl, Iryu, Iryl;
//arm and output currents of MMC
double Uxu_ref, Uxl_ref, Uyu_ref, Uyl_ref;
```

```
//voltage references of the upper and the lower MMC arms
double Ux, Uy;
//load section voltages
double Irx_ref_prev, Iry_ref_prev;
//other variables
double Irx_ref1, Iry_ref1;
//other variables
double L, Ts;
//Control variables
L = 0.003;
Ts = 0.00002778;
while (1)
{
Irx_ref1 = Irx_ref
Iry_ref1 = Iry_ref
Uxu_ref = −Ux + ((L/(2 × Ts)) × ((2 × Irx_ref1) − Irx_ref_prev + (2 × Irxu));//equation 23
Uxl_ref = +Ux − ((L/(2 × Ts)) × ((2 × Irx_ref1) − Irx_ref_prev − (2 × Irxl));//equation 24
Uyu_ref = −Uy + ((L/(2 × Ts)) × ((2 × Iry_ref1) − Iry_ref_prev + (2 × Iryu));//equation 25
Uyl_ref = +Uy − ((L/(2 × Ts)) × ((2 × Iry_ref1) − Iry_ref_prev − (2 × Iryl));//equation 26
Irx_ref_prev = Irx_ref1;
Iry_ref_prev = Iry_ref1;
while (!new_values);
```

References

1. Gazafrudi, S.M.M.; Langerudy, A.T.; Fuchs, E.F.; Al-Haddad, K. Power Quality Issues in Railway Electrification: A Comprehensive Perspective. *IEEE Trans. Ind. Electron.* **2015**, *62*, 3081–3090. [CrossRef]
2. Serrano-Jiménez, D.; Abrahamsson, L.; Castaño-Solís, S.; Sanz-Feito, J. Electrical railway power supply systems: Current situation and future trends. *Int. J. Electr. Power Energy Syst.* **2017**, *92*, 181–192. [CrossRef]
3. Krastev, I.; Tricoli, P.; Hillmansen, S.; Chen, M. Future of Electric Railways: Advanced Electrification Systems with Static Converters for ac Railways. *IEEE Electrif. Mag.* **2016**, *4*, 6–14. [CrossRef]
4. He, Z.; Zheng, Z.; Hu, H. Power quality in high-speed railway systems. *Int. J. Rail Transp.* **2016**, *4*, 71–97. [CrossRef]
5. Tanta, M.; Monteiro, V.; Sousa, T.J.C.; Martins, A.P.; Carvalho, A.S.; Afonso, J.L. Power quality phenomena in electrified railways: Conventional and new trends in power quality improvement toward public power systems. In 2018 International Young Engineers Forum (YEF-ECE), Costa da Caparica. 2018, pp. 25–30. In Proceedings of the 2018 International Young Engineers Forum (YEF-ECE), Costa da Caparica, Portugal, 4 May 2018.
6. Tanta, M.; Monteiro, V.; Exposto, B.; Pinto, J.G.; Martins, A.P.; Carvalho, A.S.; Meléndez, A.A.N.; Afonso, J.L. Simplified rail power conditioner based on a half-bridge indirect AC/DC/AC Modular Multilevel Converter and a V/V power transformer. In Proceedings of the IECON 2017—43rd Annual Conference of the IEEE Industrial Electronics Society, Beijing, China, 29 October–1 November 2017; pp. 6431–6436.
7. Hafeez, K.; Khan, S.A.; Van den Bossche, A.; Hasan, Q.U. Circulating Current Reduction in MMC-HVDC System Using Average Model. *Appl. Sci.* **2019**, *9*, 1383. [CrossRef]
8. Zhang, M.; Huang, L.; Yao, W.; Lu, Z. Circulating Harmonic Current Elimination of a CPS-PWM-Based Modular Multilevel Converter With a Plug-In Repetitive Controller. *IEEE Trans. Power Electron.* **2014**, *29*, 2083–2097. [CrossRef]
9. Xu, Q.; Ma, F.; He, Z.; Chen, Y.; Guerrero, J.M.; Luo, A.; Li, Y.; Yue, Y. Analysis and Comparison of Modular Railway Power Conditioner for High-Speed Railway Traction System. *IEEE Trans. Power Electron.* **2017**, *32*, 6031–6048. [CrossRef]
10. P, H.M.; Bina, M.T. A Transformerless Medium-Voltage STATCOM Topology Based on Extended Modular Multilevel Converters. *IEEE Trans. Power Electron.* **2011**, *26*, 1534–1545. [CrossRef]
11. Ahmed, K.H.; Aboushady, A.A. Modified half-bridge modular multilevel converter for HVDC systems with DC fault ride-through capability. In Proceedings of the IECON 2014—40th Annual Conference of the IEEE Industrial Electronics Society, Dallas, TX, USA, 29 October–1 November 2014; pp. 4676–4682.
12. Talon Louokdom, E.; Gavin, S.; Siemaszko, D.; Biya-Motto, F.; Essimbi Zobo, B.; Marchesoni, M.; Carpita, M. Small-Scale Modular Multilevel Converter for Multi-Terminal DC Networks Applications: System Control Validation. *Energies* **2018**, *11*, 1690. [CrossRef]

13. Uddin, W.; Zeb, K.; Adil Khan, M.; Ishfaq, M.; Khan, I.; ul Islam, S.; Kim, H.-J.; Park, G.S.; Lee, C. Control of Output and Circulating Current of Modular Multilevel Converter Using a Sliding Mode Approach. *Energies* **2019**, *12*, 4084. [CrossRef]
14. Ben-Brahim, L.; Gastli, A.; Trabelsi, M.; Ghazi, K.A.; Houchati, M.; Abu-Rub, H. Modular Multilevel Converter Circulating Current Reduction Using Model Predictive Control. *IEEE Trans. Ind. Electron.* **2016**, *63*, 3857–3866. [CrossRef]
15. Li, Y.; Jones, E.A.; Wang, F. Circulating Current Suppressing Control's Impact on Arm Inductance Selection for Modular Multilevel Converter. *IEEE J. Emerg. Sel. Top. Power Electron.* **2017**, *5*, 182–188. [CrossRef]
16. Matas, J.; Garcia de Vicuna, L.; Miret, J.; Guerrero, J.M.; Castilla, M. Feedback Linearization of a Single-Phase Active Power Filter via Sliding Mode Control. *IEEE Trans. Power Electron.* **2008**, *23*, 116–125. [CrossRef]
17. Moranchel, M.; Bueno, E.; Sanz, I.; Rodríguez, F.J. New Approaches to Circulating Current Controllers for Modular Multilevel Converters. *Energies* **2017**, *10*, 86. [CrossRef]
18. Li, X.; Song, Q.; Liu, W.; Xu, S.; Zhu, Z.; Li, X. Performance Analysis and Optimization of Circulating Current Control for Modular Multilevel Converter. *IEEE Trans. Ind. Electron.* **2016**, *63*, 716–727. [CrossRef]
19. Lu, M.; Hu, J.; Zeng, R.; He, Z. Fundamental-Frequency Reactive Circulating Current Injection for Capacitor Voltage Balancing in Hybrid-MMC HVDC Systems During Riding Through PTG Faults. *IEEE Trans. Power Deliv.* **2018**, *33*, 1348–1357. [CrossRef]
20. Li, J.; Konstantinou, G.; Wickramasinghe, H.R.; Pou, J.; Wu, X.; Jin, X. Impact of Circulating Current Control in Capacitor Voltage Ripples of Modular Multilevel Converters Under Grid Imbalances. *IEEE Trans. Power Deliv.* **2018**, *33*, 1257–1267. [CrossRef]
21. Tu, Q.; Xu, Z.; Xu, L. Reduced Switching-Frequency Modulation and Circulating Current Suppression for Modular Multilevel Converters. *IEEE Trans. Power Deliv.* **2011**, *26*, 2009–2017.
22. Moon, J.; Kim, C.; Park, J.; Kang, D.; Kim, J. Circulating Current Control in MMC Under the Unbalanced Voltage. *IEEE Trans. Power Deliv.* **2013**, *28*, 1952–1959. [CrossRef]
23. Qin, J.; Saeedifard, M. Predictive Control of a Modular Multilevel Converter for a Back-to-Back HVDC System. *IEEE Trans. Power Deliv.* **2012**, *27*, 1538–1547.
24. Dekka, A.; Wu, B.; Yaramasu, V.; Fuentes, R.L.; Zargari, N.R. Model Predictive Control of High-Power Modular Multilevel Converters—An Overview. *IEEE J. Emerg. Sel. Top. Power Electron.* **2019**, *7*, 168–183. [CrossRef]
25. Cortes, P.; Kazmierkowski, M.P.; Kennel, R.M.; Quevedo, D.E.; Rodriguez, J. Predictive Control in Power Electronics and Drives. *IEEE Trans. Ind. Electron.* **2008**, *55*, 4312–4324. [CrossRef]
26. Luo, A.; Wu, C.; Shen, J.; Shuai, Z.; Ma, F. Railway Static Power Conditioners for High-speed Train Traction Power Supply Systems Using Three-phase V/V Transformers. *IEEE Trans. Power Electron.* **2011**, *26*, 2844–2856. [CrossRef]
27. Tanta, M.; Afonso, J.A.; Martins, A.P.; Carvalho, A.S.; Afonso, J.L. Comprehensive Study for a Rail Power Conditioner Based on a Single–Phase Full–Bridge Back–to–Back Indirect Modular Multilevel Converter. In *Transactions on Engineering Technologies*; Ao, S.-I., Gelman, L., Kim, H.K., Eds.; Springer: Singapore, 2019; pp. 263–279.
28. Monteiro, V.D.F. *Development of Bidirectional Charging Systems for Electric Vehicles with New Modes of Operation for Smart Grid, in Portuguese: Desenvolvimento de sistemas de carregamento bidirecionais para veículos elétricos com novos modos de operação para Smart Grids*; University of Minho: Braga, Portugal, 2016.
29. Chen, M.; Sun, J. Feedforward current control of boost single-phase PFC converters. *IEEE Trans. Power Electron.* **2006**, *21*, 338–345. [CrossRef]
30. Tan, S.; Lai, Y.M.; Tse, C.K.; Wu, C.K. A pulsewidth modulation based integral sliding mode current controller for boost converters. In Proceedings of the 2006 37th IEEE Power Electronics Specialists Conference, Jeju, Korea, 18–22 June 2006; pp. 1–7.
31. Orts-Grau, S.; Gimeno-Sales, F.J.; Abellan-Garcia, A.; Segui-Chilet, S.; Alfonso-Gil, J.C. Improved Shunt Active Power Compensator for IEEE Standard 1459 Compliance. *IEEE Trans. Power Deliv.* **2010**, *25*, 2692–2701. [CrossRef]

32. Tanta, M.; Pinto, G.; Monteiro, V.; Martins, A.P.; Carvalho, A.S.; Afonso, J.L. A Comprehensive Comparison of Rail Power Conditioners Based on Two-level Converters and a V/V Power Transformer in Railway Traction Power Systems. In Proceedings of the 7th Transport Research Arena (TRA 2018), Vienna, Austria, 16–19 April 2018; pp. 1–10.
33. Karimi-Ghartemani, M.; Karimi, H.; Iravani, M.R. A magnitude/phase-locked loop system based on estimation of frequency and in-phase/quadrature-phase amplitudes. *IEEE Trans. Ind. Electron.* **2004**, *51*, 511–517. [CrossRef]